

Honeycombs of triangles and magnetic frustration in SrL_2O_4 ($L=\text{Gd, Dy, Ho, Er, Tm, and Yb}$)H. Karunadasa,¹ Q. Huang,² B. G. Ueland,³ J. W. Lynn,² P. Schiffer,³ K. A. Regan,¹ and R. J. Cava¹¹*Department of Chemistry, Princeton University, Princeton, New Jersey 08544, USA*²*NIST Center for Neutron Research, National Institute of Standards and Technology, Gaithersburg, Maryland 20899, USA*³*Department of Physics and Materials Research Institute, The Pennsylvania State University, University Park, Pennsylvania 16802, USA*

(Received 21 September 2004; published 19 April 2005)

The crystal structures, magnetic order, and susceptibility have been investigated for magnetically frustrated SrDy_2O_4 , SrHo_2O_4 , SrEr_2O_4 , SrTm_2O_4 , and SrYb_2O_4 . Powder neutron-diffraction structural refinements reveal columns of LO_6 octahedra that run along one crystallographic direction, with Sr-O polyhedra in the interstices. The lanthanide sublattice displays multiple triangular interconnections: one-dimensional strings form the backbones of four types of chains of lanthanide triangles sharing edges arranged in a honeycomb pattern. This crystal structure produces strong geometric frustration for the magnetic system that is evidenced in both magnetic susceptibility and neutron-scattering data at low temperatures. The susceptibility measurements for the series, including SrGd_2O_4 for which data are also reported, lack the sharp features characteristic of three-dimensional long-range magnetic ordering. Metamagnetic behavior is observed in the magnetization vs applied field data at 1.8 K for the cases of $L=\text{Dy, Er, and Ho}$. Magnetic neutron-scattering studies for the Dy and Er materials show only very broad magnetic scattering at low temperatures, while the Ho system exhibits long-range two-dimensional order. Any magnetic scattering in the Tm and Yb compounds, if present, was too weak to be detected in these measurements.

DOI: 10.1103/PhysRevB.71.144414

PACS number(s): 75.40.Cx, 61.12-q

I. INTRODUCTION

Long-range magnetic ordering of strongly interacting spins at low temperatures can be frustrated by triangular geometric arrangements in a crystal lattice. Geometrical frustration in magnetic materials is an active area of experimental and theoretical experimental research. A large number of different ground states have been discovered, including glassy states in the limit of low disorder, a “spin ice” state that mimics the low-temperature behavior of frozen water, and numerous spin-liquid-like states.¹⁻⁵ This field has largely been driven by the discovery of interesting materials in which frustration plays an important role. Geometrically simple, triangle-based lattices such as the *kagomé* and pyrochlore lattices have been actively studied, but more complex lattices, such as the “*kagomé staircase*”^{6,7} are now beginning to be explored to test how variations in geometry influence the frustration. Here we report the crystal structures and basic magnetic characterization of a different lattice geometry for frustrated magnetic materials, in materials of formula SrL_2O_4 for $L=\text{Gd, Dy, Ho, Er, Tm, and Yb}$. The magnetic lanthanide sublattice in these materials consists completely of triangles—chains of edge-shared lanthanide triangles in a honeycomblike arrangement. SrL_2O_4 compounds with this structure type have been previously reported,⁸⁻¹¹ and the structures have previously been determined by x-ray diffraction for the cases of $L=\text{Y, Yb, and Tb}$.¹²⁻¹⁴ SrEu_2O_4 has had its magnetic susceptibility reported previously, and $L=\text{Eu, Gd, and Y}$ (Ref. 15) have been characterized spectroscopically. Here we show that these materials display the signatures of geometrically frustrated magnetic systems both through magnetic susceptibility and neutron-scattering measurements.

II. EXPERIMENT

Two-gram samples of the Gd, Dy, Ho, Er, Tm, and Yb analogs of SrL_2O_4 were prepared from high-purity starting materials of SrCO_3 , Gd_2O_3 , Dy_2O_3 , Er_2O_3 , Ho_2O_3 , Tm_2O_3 , and Yb_2O_3 . Stoichiometric mixtures of the powders were mixed in an agate mortar and heated in air in dense, high-purity Al_2O_3 crucibles. The samples were heated at 1500 °C for a total of 48 h with several intermediate grindings.

The crystal structures of SrL_2O_4 were determined at ambient temperature by powder neutron diffraction, at the NIST

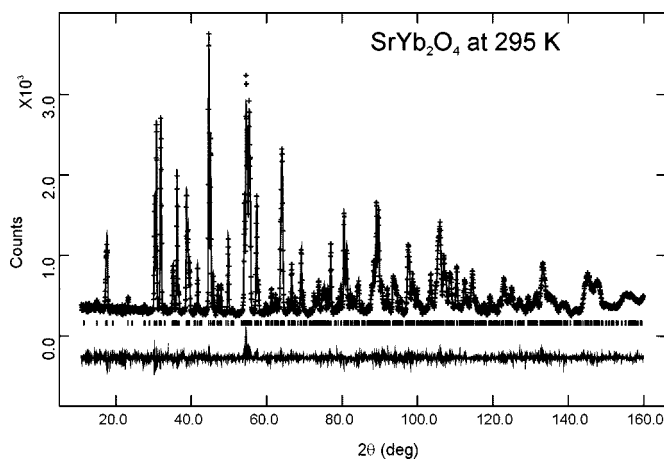


FIG. 1. Neutron powder-diffraction pattern of SrYb_2O_4 at ambient temperature. Upper curve: data and fit, short vertical lines, calculated peak positions. Lower curve: difference between observed and calculated pattern.

TABLE I. Structural parameters for SrL_2O_4 ($L=\text{Dy, Ho, Er, Tm, and Yb}$) at room temperature. Space group: Pnm . All atoms are in site $4c$ ($x, y, 1/4$).

	($L=$)	Dy	Ho	Er	Tm	Yb
	a (Å)	10.0884(4)	10.0674(3)	10.0451(4)	10.0040(4)	9.9921(2)
	b (Å)	11.9427(5)	11.9104(4)	11.8676(5)	11.8163(5)	11.7736(3)
	c (Å)	3.4289(1)	3.4087(1)	3.3899(1)	3.3769(1)	3.35768(8)
	V (Å ³)	413.12(4)	408.72(4)	404.11(5)	399.19(5)	395.00(3)
Sr	x	0.7515(5)	0.7525(2)	0.7539(3)	0.7537(3)	0.7528(2)
	y	0.6487(5)	0.6498(2)	0.6505(3)	0.6500(2)	0.6503(2)
	B (Å ²)	0.79(9)	0.90(5)	0.72(5)	0.74(5)	0.81(3)
$R(1)$	x	0.4242(3)	0.4233(2)	0.4228(3)	0.4220(3)	0.4217(2)
	y	0.1110(2)	0.1104(2)	0.1100(2)	0.1094(2)	0.1090(1)
	B (Å ²)	0.52(6)	0.51(3)	0.74(4)	0.63(5)	0.59(2)
$R(2)$	x	0.4208(3)	0.4221(2)	0.4231(3)	0.4247(3)	0.4253(1)
	y	0.6122(2)	0.6126(2)	0.6120(2)	0.6123(2)	0.6123(1)
	B (Å ²)	0.44(6)	0.42(3)	0.68(4)	0.59(5)	0.59(2)
O(1)	x	0.2105(7)	0.2118(3)	0.2107(3)	0.2103(3)	0.2102(3)
	y	0.1766(6)	0.1755(3)	0.1742(3)	0.1728(3)	0.1716(2)
	B (Å ²)	0.8(1)	0.94(5)	0.67(6)	0.67(6)	0.65(4)
O(2)	x	0.1263(6)	0.1254(3)	0.1247(3)	0.1243(3)	0.1234(2)
	y	0.4822(6)	0.4810(3)	0.4802(3)	0.4800(3)	0.4802(2)
	B (Å ²)	0.70(10)	0.84(5)	0.82(6)	0.79(6)	0.91(5)
O(3)	x	0.5135(7)	0.5142(3)	0.5148(4)	0.5162(3)	0.5176(3)
	y	0.7843(6)	0.7840(2)	0.7837(3)	0.7841(2)	0.7839(2)
	B (Å ²)	0.90(10)	0.88(5)	0.88(6)	0.80(6)	0.82(4)
O(4)	x	0.4260(8)	0.4254(3)	0.4238(4)	0.4252(3)	0.4247(3)
	y	0.4232(4)	0.4223(2)	0.4223(2)	0.4230(2)	0.4239(2)
	B (Å ²)	0.70(10)	0.82(5)	0.52(6)	0.66(6)	0.79(4)
	R_p (%)	4.17	3.42	3.84	3.78	3.44
	R_{wp} (%)	5.07	4.22	4.82	4.70	4.20
	χ^2	0.79	0.90	0.81	0.83	0.92

TABLE II. Selected bond distances (Å) in SrL_2O_4 ($L=\text{Dy, Ho, Er, Tm, and Yb}$) at room temperature.

	($L=$)	Dy	Ho	Er	Tm	Yb
Sr-O(1)	×2	2.728(8)	2.713(3)	2.707(4)	2.714(4)	2.711(3)
Sr-O(2)	×2	2.627(7)	2.616(2)	2.601(3)	2.588(3)	2.591(3)
Sr-O(3)		2.896(9)	2.883(4)	2.875(4)	2.856(4)	2.828(3)
Sr-O(3)		2.761(9)	2.750(4)	2.735(5)	2.738(4)	2.757(4)
Sr-O(4)	×2	2.624(8)	2.617(3)	2.609(4)	2.608(3)	2.594(3)
$R(1)$ -O(1)		2.294(8)	2.266(4)	2.262(4)	2.246(4)	2.238(3)
$R(1)$ -O(2)	×2	2.359(6)	2.350(3)	2.340(3)	2.324(3)	2.306(2)
$R(1)$ -O(2)		2.322(7)	2.308(4)	2.294(4)	2.283(4)	2.272(3)
$R(1)$ -O(3)	×2	2.214(5)	2.210(2)	2.203(3)	2.195(2)	2.186(2)
$R(2)$ -O(1)	×2	2.299(5)	2.299(2)	2.286(3)	2.277(3)	2.267(2)
$R(2)$ -O(3)		2.257(7)	2.242(4)	2.237(4)	2.227(4)	2.221(3)
$R(2)$ -O(4)		2.258(6)	2.267(3)	2.251(4)	2.237(3)	2.218(2)
$R(2)$ -O(4)	×2	2.346(6)	2.331(3)	2.324(3)	2.298(3)	2.291(2)

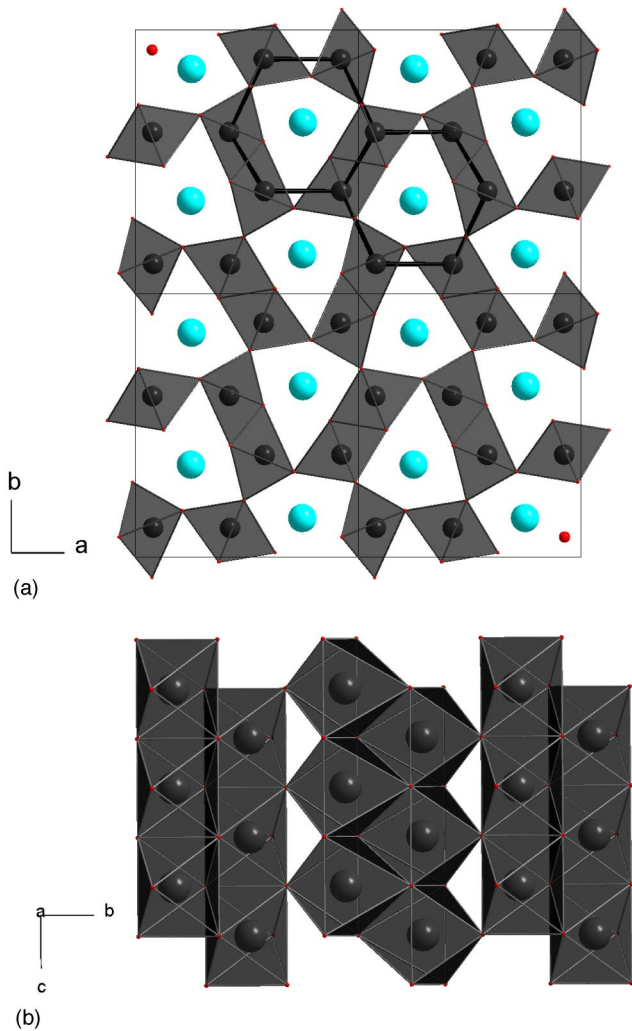


FIG. 2. (Color online) (a) The crystal structure of SrDy₂O₄ shown as an arrangement of LO₆ octahedra and isolated Sr atoms in channels, viewed down the crystallographic *c* axis. (b) The arrangement of LO₆ octahedra perpendicular to *c* showing both the double-row columns of octahedra, and the manner in which those columns share corner oxygens with each other.

Center for Neutron Research, on the high-resolution powder neutron diffractometer, with monochromatic neutrons of wavelength 1.5402 Å produced by a Cu(311) monochromator. Data were collected at ambient temperature between 3° and 168° diffraction angles with a step size of 0.05°. Collimators with horizontal divergences of 15', 20', and 7' of arc were employed before and after the monochromator, and after the sample, respectively. Structure refinement by the Rietveld method was carried out with the program GSAS.¹⁶ The neutron-scattering amplitudes employed in the refinement were as specified in the program. Statistical uncertainties quoted in all the neutron results represent one standard deviation.

Magnetic susceptibilities were measured on powder samples between 2 and 300 K in a Quantum Design MPMS magnetometer. The applied field was 50 Oe. Field-dependent magnetization measurements were carried out at 1.8 K up to

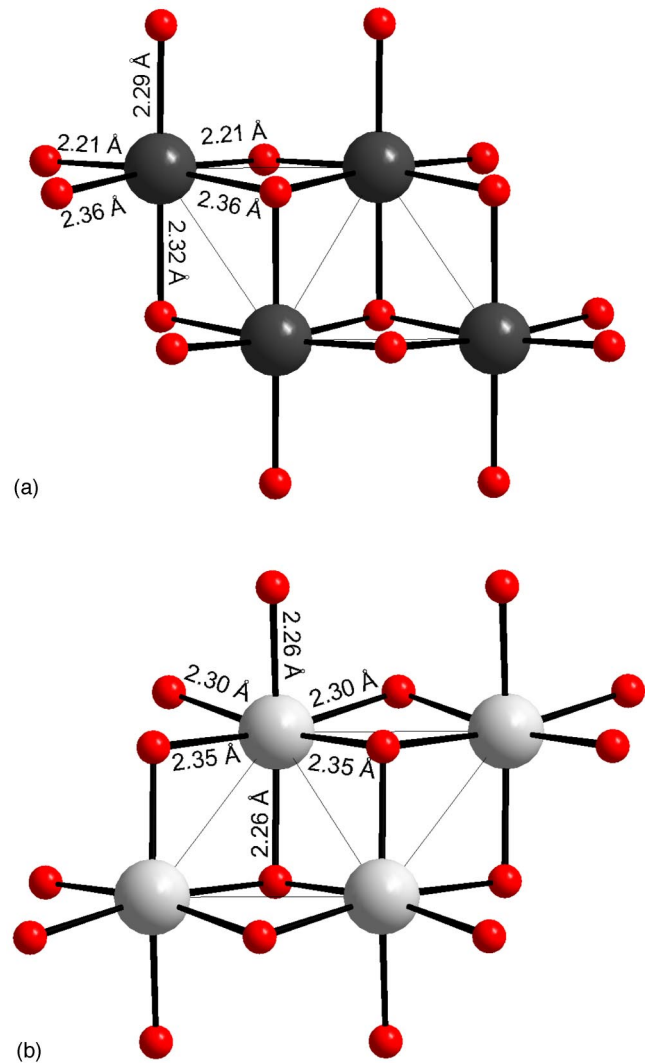


FIG. 3. (Color online) The geometries of the LO₆ octahedra in the double-row columns, for (a) L(1), and (b) L(2). The lanthanide-oxygen distances are shown for the case of SrDy₂O₄. L(1) shown as larger dark circles, L(2) shown as larger lighter circles, oxygen as small black circles.

a field of 7 T. Magnetic neutron scattering was performed with neutrons of wavelength 2.47 Å on the BT-7 triple-axis spectrometer at the NIST Center for Neutron Research, employing a pyrolytic graphite filter and analyzer.

III. CRYSTAL STRUCTURES

A representative neutron-diffraction pattern is shown in Fig. 1 for SrYb₂O₄. The initial structural model was taken from the structure of SrY₂O₄.¹² The fit to the structural model is excellent. Our results for SrYb₂O₄ are in agreement with those from x-ray analysis.¹³ All parameters in the fits for all lanthanides were well behaved, and the refined structural parameters for all lanthanides studied are presented in Table I. Selected metal-oxygen bond distances are presented in Table II.

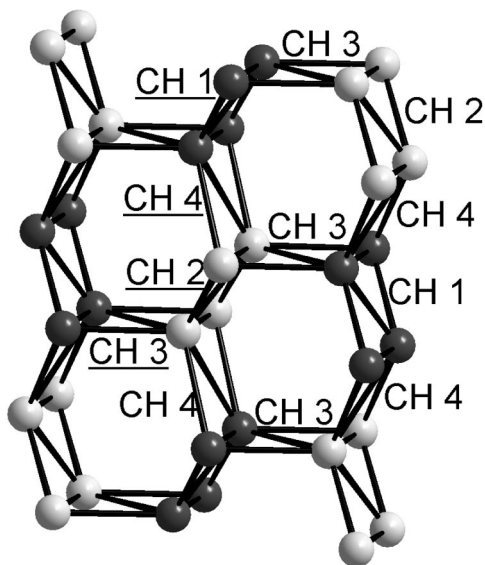


FIG. 4. Detailed view of the magnetic atom sublattice in the “honeycomb” direction in SrDy₂O₄, showing the four lanthanide chains running perpendicular to the honeycomb net. Lines connect near neighbor lanthanides. L(1) shown as dark circles, L(2) shown as lighter circles.

Interpretation of the magnetic properties of these materials requires the consideration of several different aspects of the magnetic atom sublattice within the overall structure. The full crystal structure for SrDy₂O₄ is shown in Fig. 2(a), in a

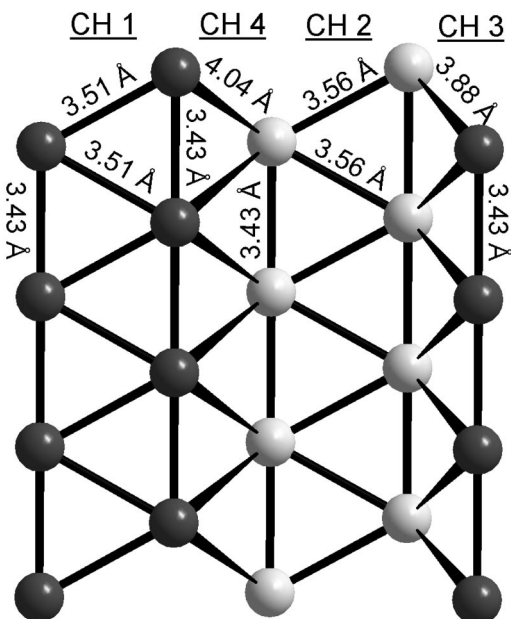


FIG. 5. Side view of the lanthanide chains, running parallel to the crystallographic *c* axis. L(1) shown as dark circles, L(2) shown as lighter circles. Lines connect lanthanide near neighbors. Interlanthanide distances are shown for the case of Dy. The primary chains, CH1 and CH2, have shorter *L-L* separations, and the secondary, or connecting chains, CH3 and CH4, have longer *L-L* distances. The shorter *L-L* distances along the spines of the chains are also seen.

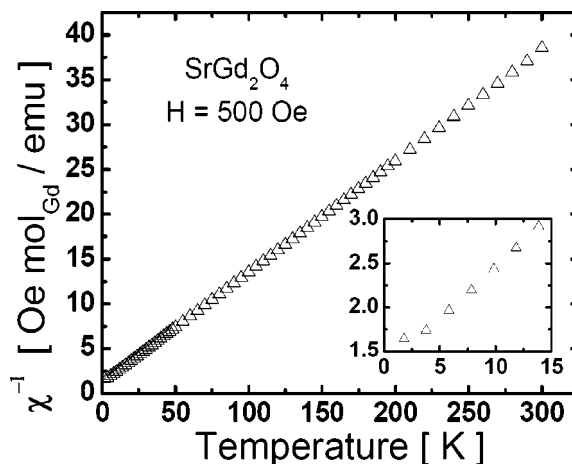


FIG. 6. The temperature dependence of the inverse magnetic susceptibility for SrGd₂O₄ between 320 and 2 K. Data taken on cooling in an applied field of 500 Oe. Inset: detail of the inverse susceptibility in the low-temperature region.

view along the crystallographic *c* axis. The LO₆ octahedra are shown in a polyhedral representation. The nonmagnetic Sr atoms fill columnar cavities in the network of edge and corner shared LO₆ octahedra. The honeycomb arrangement of the lanthanides is outlined by bold lines. Double rows of edge-shared LO₆ octahedra form the walls of the honeycomb, in infinite columns running perpendicular to the *a-b* plane, and are shown in Fig. 2(b). Each double-row column contains only one of the two crystallographically independent *L* atoms. These columns share corner oxygens with each other. The views presented in Figs. 2(a) and 2(b) emphasize the structural analogy of SrL₂O₄ to CaFe₂O₄.¹⁷

The details of the *L-O* coordination and the geometrical relationship among lanthanides in the chains are shown in Figs. 3(a) and 3(b), using data for the specific case of SrDy₂O₄. The *L-O* coordination polyhedra in all cases are slightly irregular; both in their bond angles and bond distances (see Table II). The *L-O* distances within the octahedra

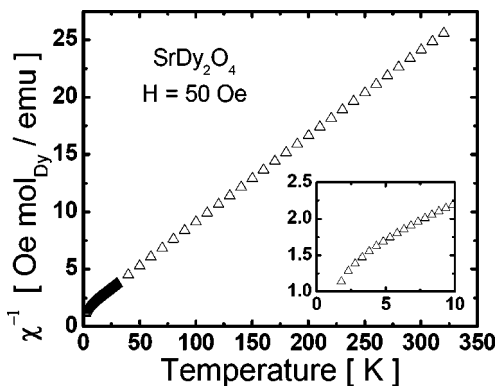


FIG. 7. The temperature dependence of the inverse magnetic susceptibility for SrDy₂O₄ between 320 and 2 K. Data taken on cooling in an applied field of 50 Oe. Inset: detail of the inverse susceptibility in the low-temperature region.

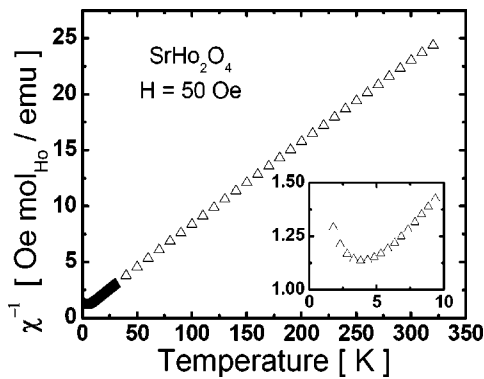


FIG. 8. The temperature dependence of the inverse magnetic susceptibility for SrHo_2O_4 between 320 and 2 K. Data taken on cooling in an applied field of 50 Oe. Inset: detail of the inverse susceptibility in the low-temperature region.

are of particular interest, because, for example, Dy is known to display Ising spin character when in a strong axial crystal field, as is found in the pyrochlore structure type.¹⁸ In the present case, there are differences in Dy-O bond lengths of up to 0.15 Å for Dy1, and up to 0.09 Å for Dy2. Although substantially smaller than the differences in the pyrochlores (which are about 0.3 Å), these may nonetheless be sufficient to result in Ising-like behavior.

For lanthanides in insulating materials, direct exchange is the dominant mechanism for magnetic coupling. Therefore the arrangement of the lanthanides is the relevant part of the structure to consider when interpreting magnetic properties. The arrangement of the lanthanides for the SrL_2O_4 compounds is shown in Figs. 4 and 5. Nearest neighbor L - L distances are shown as connecting lines. The lanthanide arrangement is seen to consist entirely of edge-shared isosceles triangles, forming chains running parallel to the crystallographic c axis. The chains, designated as chains 1–4, connect to each other in a honeycomb pattern in the perpendicular plane. (The separations presented in Fig. 5 are for SrDy_2O_4 as an example.) Chains 1 and 2 are within the double-row columns of edge-shared LO_6 octahedra, and have the closer

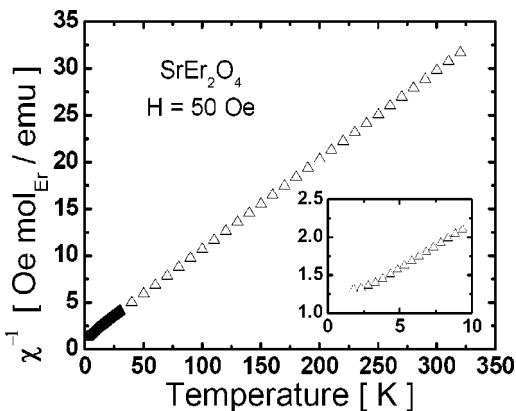


FIG. 9. The temperature dependence of the inverse magnetic susceptibility for SrEr_2O_4 between 320 and 2 K. Data taken on cooling in an applied field of 50 Oe. Inset: detail of the inverse susceptibility in the low-temperature region.

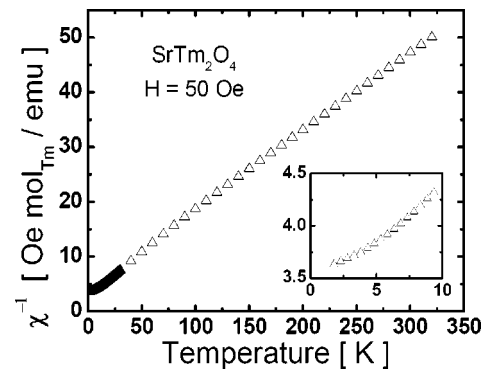


FIG. 10. The temperature dependence of the inverse magnetic susceptibility for SrTm_2O_4 between 320 and 2 K. Data taken on cooling in an applied field of 50 Oe. Inset: detail of the inverse susceptibility in the low-temperature region.

L - L distances. For SrDy_2O_4 , the triangles in these chains show 3.43-Å L - L distances along the spines of the chains (the crystallographic c axis) and 3.51 Å (chain 1) or 3.56 Å (chain 2) between the lanthanides in parallel spines. The somewhat shorter distance along the spines of the chains may result in some degree of one-dimensional character in the magnetic interactions, and chains 1 and 2 have approximately equivalent geometries. The L - L distances across the interconnecting chains, 3 and 4, are considerably longer (about 0.4 Å) than those in the primary chains, because they derive from the corner sharing rather than the edge sharing of LO_6 octahedra [3.90 Å (chain 3) and 4.04 Å (chain 4), respectively, for SrDy_2O_4]. Therefore the magnetic coupling across these interconnecting chains will be weaker than that within the primary chains. The coupling across these interconnecting chains is also expected to be frustrated, however, due to the triangular motif.

IV. MAGNETIC PROPERTIES

The magnetic susceptibilities for powder samples of the SrL_2O_4 compounds are presented in Figs. 6–11. For all but

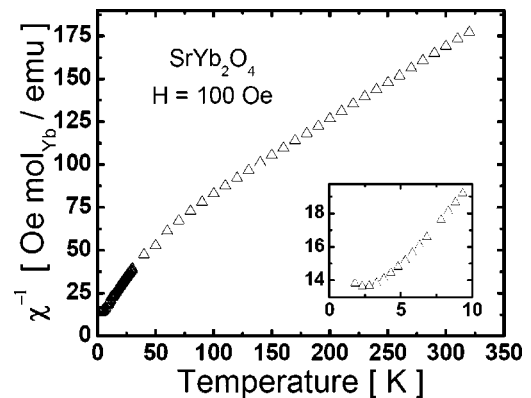


FIG. 11. The temperature dependence of the inverse magnetic susceptibility for SrYb_2O_4 between 320 and 2 K. Data taken on cooling in an applied field of 100 Oe. Inset: detail of the inverse susceptibility in the low-temperature region.

TABLE III. Magnetic parameters for SrLn_2O_4 obtained from fits to the magnetic susceptibilities between 150 and 320 K (18 points), or, in the case of Gd, between 100 and 300 K (31 points). Values presented are effective moment (p) in bohr magnetons (μ_B), expected moment (p_{exp}) from Ref. 19, Curie Weiss theta (θ_W), and goodness of fit (R^2). Numbers in parentheses represent one standard deviation.

Compound	p (μ_B)	p_{exp}	θ_W	R^2
SrGd_2O_4	8.02(2)	7.9	-9.0(6)	0.99998
SrDy_2O_4	10.35(1)	10.6	-22.9(5)	1.0
SrHo_2O_4	10.50(1)	10.4	-16.9(5)	0.99994
SrEr_2O_4	9.176(3)	9.5	-13.5(2)	0.99999
SrTm_2O_4	7.51(1)	7.3	-33.8(6)	0.99999
SrYb_2O_4	4.348(6)	4.5	-99.4(7)	0.99997

the Yb analog, the magnetic susceptibilities follow Curie Weiss behavior from approximately 50 to 300 K. In the Yb case, substantial curvature sets in by 150 K. The parameters of the fits for the Curie-Weiss regions are presented in Table III. The effective moments are consistent with those expected for the lanthanides. In all cases, θ_W is negative, ranging from a minimum of -13 K for $L=\text{Er}$, to a maximum of -99 K for $L=\text{Yb}$.

The insets to Figs. 6–11 show the low-temperature susceptibilities in detail. None of the samples show the sharp features associated with long-range three-dimensional magnetic ordering despite the fact that the data reach temperatures well below θ_W . Such suppression is typical of geometrically frustrated magnets, and is consistent with the triangle-based geometry of these compounds. The Er, Yb, Tm, and Ho variants show the onset of upward curvature in the inverse susceptibility plots at low temperatures, at approximately 2, 3, 2, and 4 K, respectively. The change in slope is gradual, not as sharp as would be expected for long-range antiferromagnetic ordering, and suggests the onset of short-range ordering transitions. The Dy case is of particular interest, as the curvature at low temperatures is downward rather

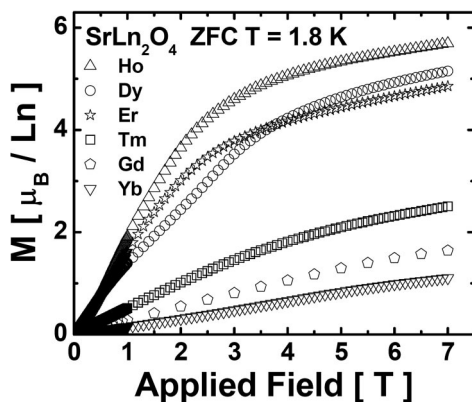


FIG. 12. The magnetization for SrLn_2O_4 materials as a function of applied field at 1.8 K. Zero-field cooling.

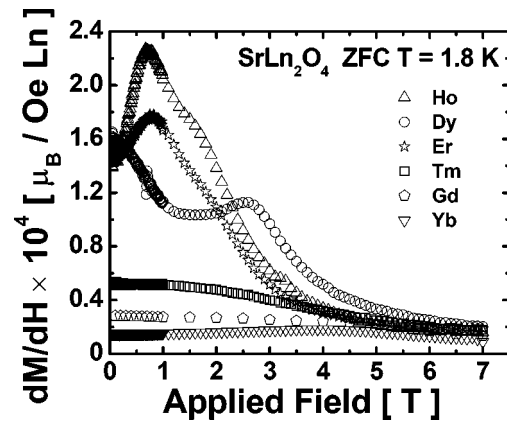


FIG. 13. The derivatives, dM/dH of the magnetization data in Fig. 12, as a function of applied field.

than upward in the inverse chi plots, indicating the presence of residual paramagnetic behavior.^{20,21} For the Gd case, there is little indication of curvature in the inverse chi plot (Fig. 6) at high temperatures. The susceptibility shows weak signs of an approaching magnetic transition below 2 K.

The field-dependent magnetizations for the SrLn_2O_4 materials up to fields of 7 T at 1.8 K are shown in Fig. 12. For the cases of Gd, Tm, and Yb, broadly curving behavior is seen in the whole field range, with some tendency toward saturation, though not clearly so. The derivatives of the magnetizations for these materials, shown in Fig. 13, show dM/dH at all H to be only weakly monotonically changing. Therefore very little ferromagnetic character is present in whatever form of ordering has taken place in these materials by 1.8 K. For the cases of Ho, Dy, and Er, on the other hand, the magnetization is larger at high applied fields and shows clear indications of reaching saturation. The saturated moments are, however, substantially lower than the local moments seen in the high-temperature magnetic susceptibilities, indicative of the fact that the spins cannot all be aligned with the field up to 7 T.

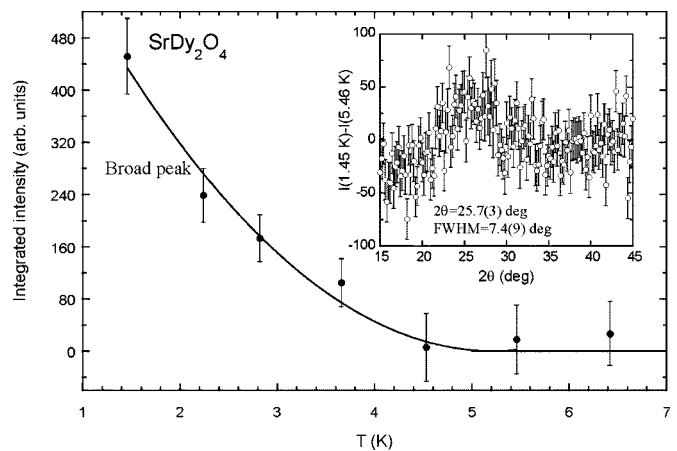


FIG. 14. A broad magnetic peak is observed below ~ 5 K in SrDy_2O_4 (inset), indicating that short-range magnetic order develops at low temperatures in this system.

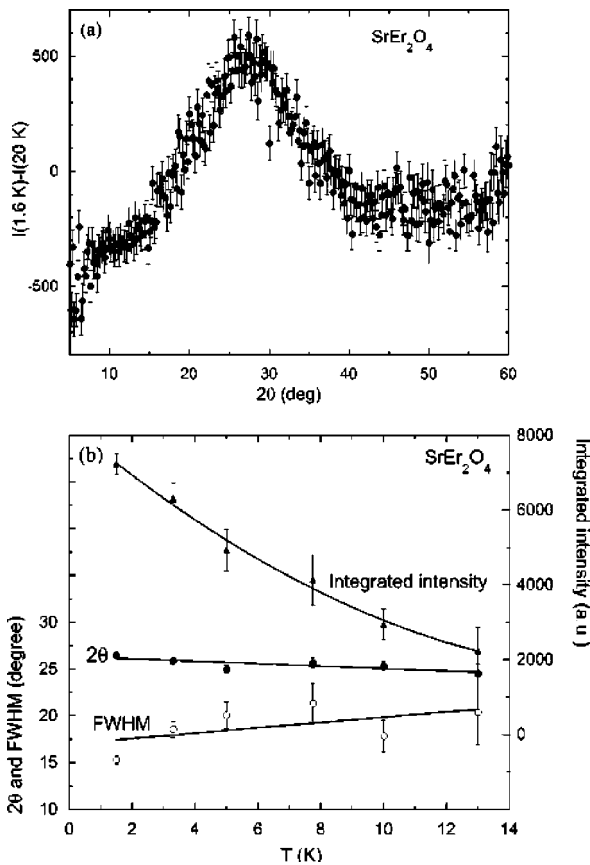


FIG. 15. (a) A very broad peak showing the short-range magnetic order develops below ~ 20 K in SrEr_2O_4 ; (b) integrated intensity, full width at half maximum (FWHM), and position of the broad peak as a function of temperature.

For these materials, the derivatives dM/dH all show a double peak behavior, indicating the presence of metamagnetism. This suggests that rich field and temperature-dependent magnetic phase diagrams may be accessible for future study of these materials under common experimental conditions.

V. MAGNETIC NEUTRON SCATTERING

No evidence of three-dimensional long-range magnetic order was observed between 300 and 1.5 K for any of the five samples studied by neutron scattering (SrGd_2O_4 was not studied). As shown in Figs. 14 and 15, however, a broad peak was observed at low temperature for SrDy_2O_4 and SrEr_2O_4 near the (020) reflection, with peak widths of 7.4° and 18° , respectively. The instrumental width is about 1° at this diffraction angle under the experimental conditions employed. This observation indicates the presence of short-range magnetic order in these systems. The broad peak disappears above ~ 5 K for SrDy_2O_4 and ~ 20 K for SrEr_2O_4 .

Figures 16 and 17 show the magnetic ordering behavior observed by neutron scattering in SrHo_2O_4 . Two magnetic transitions were found. Similar to what is found in the Dy

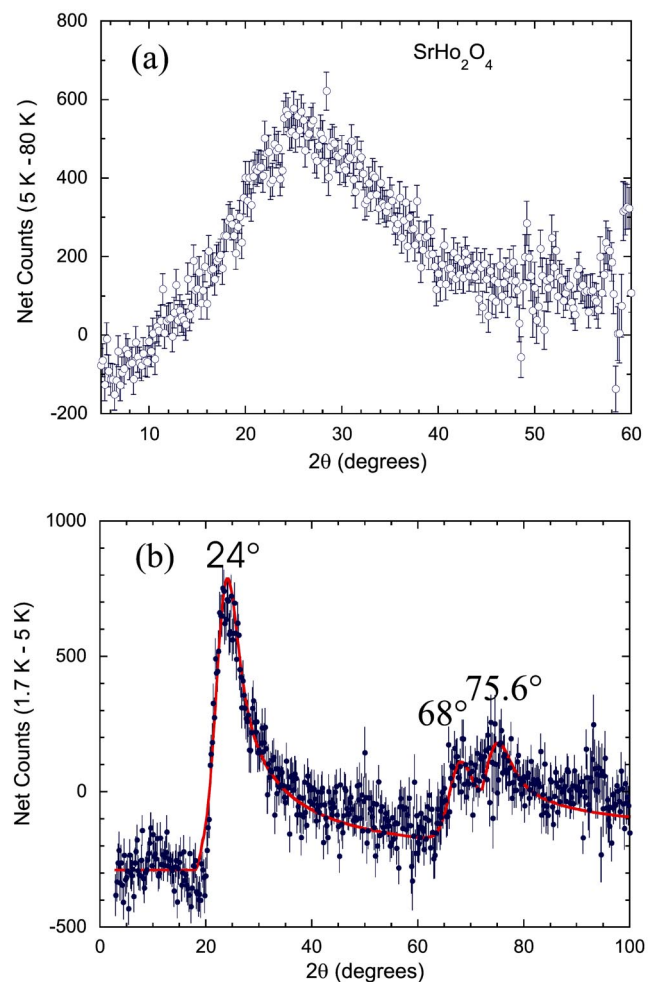


FIG. 16. (Color online) (a) Broad distribution of magnetic scattering at intermediate temperatures, indicating the development of short-range correlations in SrHo_2O_4 . This scattering begins to develop below ~ 40 K. (b) The magnetic scattering at low temperatures, indicating the development of two-dimensional long-range magnetic order. The solid curve is a fit assuming long-range order within the ab plane, and no correlations between planes.

and Er cases, below ~ 40 K a broad peak, due to short-range magnetic ordering, was observed. The intensity measured as a function of temperature at the position of the broad peak ($2\theta = 23.6^\circ$) shows a change in its rate of increase below ~ 4 K [Fig. 17(b)]. Figure 14(a) shows the magnetic scattering peak that characterizes the magnetic state that develops above 5 K. The character of the scattering changes below 5 K. Figure 16(b) shows the magnetic intensity obtained from subtracting the data taken at 5.05 K from the data collected at 1.72 K. The shape is characteristic of what is seen for two-dimensional (2D) ordering. The solid curve is a fit to 2D scattering theory, assuming long-range order within a plane, and no correlations perpendicular to the plane.²² The three peaks of magnetic origin at $\sim 24^\circ$, 68° , and 75.6° are close to the positions expected for (02), (34), and (50) rods in reciprocal space, respectively, with intensities due to ordering in the a - b plane. The splitting between the 68° and 75.6° peaks is due to the structural anisotropy of the system. No evidence

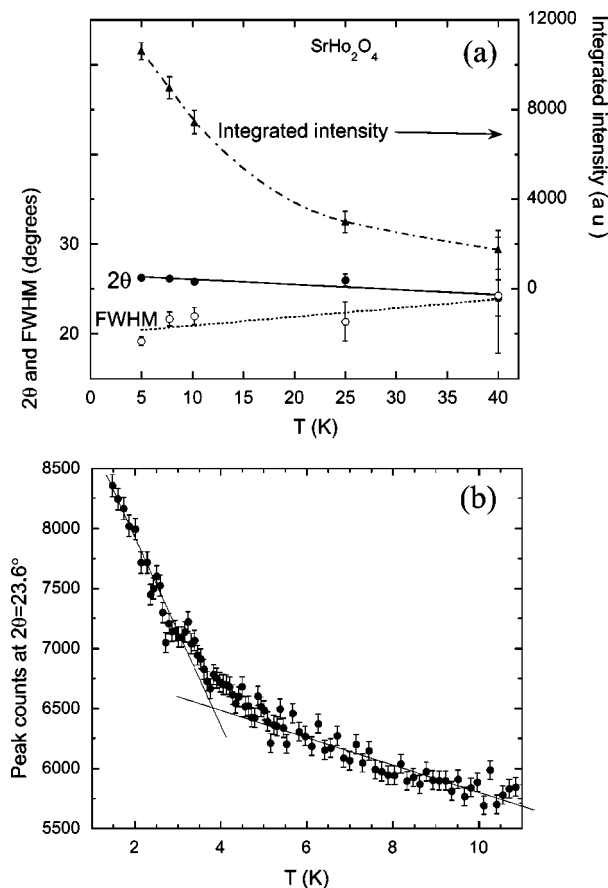


FIG. 17. (a) Plots of the integrated intensity, position, and FWHM as a function of temperature for the short-range order correlations in SrHo₂O₄. (b) Intensity vs temperature at the 2D (02) peak position. The change in slope around 4 K indicates a crossover from short-range magnetic correlations to 2D long-range order.

of magnetic ordering was observed in either SrYb₂O₄ or SrTm₂O₄. In both cases this may be due to the low magnetic moments of the heavy lanthanides Tm and Yb.

VI. CONCLUSIONS

The crystal structures and elementary magnetic characterization of a different family of geometrically frustrated magnetic materials has been described. The crystal structures contain a magnetic sublattice with several levels of low dimensionality and frustration. One-dimensional strings of lanthanides separated by approximately 3.4 Å form the spines of two nearly equivalent chains made of edge-shared isosceles triangles (the other two sides are approximately 3.5 Å) running in one crystallographic direction. These chains are themselves connected by secondary chains of isosceles triangles that, due to their longer sides (near 4 Å) should result in weaker but also frustrated coupling between the primary chains. The chains are arranged in a honeycomb pattern. The complexities of the resulting magnetic states at low temperatures, which differ from one lanthanide to another, are suggested by both the magnetic susceptibility data and the magnetic neutron-scattering data. Substantial opportunities for further characterization are suggested, and the growth of single crystals of these materials would be of great interest.

ACKNOWLEDGMENTS

This work was partially supported by the National Science Foundation, Grant No. DMR 0244254 and by Army Research Office PECASE Grant No. DAAD19-01-1-0021. Identification of commercial equipment in the text is not intended to imply recommendation or endorsement by the National Institute of Standards and Technology.

- ¹A. P. Ramirez, in *Handbook of Magnetic Materials*, edited by K. J. H. Buschow (New Holland, New York, 2001), Vol. 13.
- ²J. E. Greedan, *J. Mater. Chem.* **11**, 37 (2001).
- ³R. Moessner, *Can. J. Phys.* **79**, 1283 (2001).
- ⁴P. Schiffer and A. P. Ramirez, *Comments Condens. Matter Phys.* **18**, 21 (1996).
- ⁵Proceedings of the Highly Frustrated Magnetism 2003 Conference [*J. Phys.: Condens. Matter* **16**, S553 (2004)].
- ⁶N. Rogado, G. Lawes, D. A. Huse, A. P. Ramirez, and R. J. Cava, *Solid State Commun.* **124**, 229 (2002).
- ⁷G. Lawes, M. Kenzelmann, N. Rogado, K. H. Kim, G. A. Jorge, R. J. Cava, A. Aharony, O. Entin-Wohlman, A. B. Harris, T. Yildirim, Q. Z. Huang, S. Park, C. Broholm, and A. P. Ramirez, *Phys. Rev. Lett.* **93**, 247201 (2004).
- ⁸L. M. Lopato and A. E. Kuschevskii, *Ukrainskii Khimicheskii Zhurnal (Russian edition)* **39**, 7 (1971).
- ⁹J. G. Pepin, *J. Appl. Crystallogr.* **14**, 70 (1981).
- ¹⁰C. Q. Han, X. L. Chen, J. K. Liang, Q. L. Liu, Y. Chen, and G. H. Rao, *J. Alloys Compd.* **309**, 95 (2000).
- ¹¹S. Arul Antony, K. S. Nagaraja, G. L. N. Reddy, and O. M. Sreedharan, *Mater. Lett.* **51**, 414 (2001).

- ¹²H. Muller-Buschbaum, *Z. Anorg. Allg. Chem.* **358**, 136 (1968).
- ¹³H. Muller-Buschbaum and R. von Schenck, *Z. Anorg. Allg. Chem.* **377**, 70 (1970).
- ¹⁴E. Paletta and H. Muller-Buschbaum, *J. Inorg. Nucl. Chem.* **30**, 1425 (1968).
- ¹⁵M. Taibi, E. Antic-Fidancev, J. Aride, M. Lemaitre-Blaise, and P. Porcher, *J. Phys.: Condens. Matter* **5**, 5201 (1993).
- ¹⁶A. C. Larson and R. B. Von Dreele, *General Structure Analysis System*, Report No. LAUR086-748, Los Alamos National Laboratory, Los Alamos, New Mexico, 1990.
- ¹⁷P. M. Hill, H. S. Peiser, and J. R. Rait, *Acta Crystallogr.* **9**, 981 (1956).
- ¹⁸S. Rosenkranz, A. P. Ramirez, A. Hayashi, R. J. Cava, R. Siddharthan, and B. B. Shastry, *J. Appl. Phys.* **87**, 5914 (2000).
- ¹⁹C. Kittel, *Introduction to Solid State Physics* (John Wiley and Sons, New York, 1992), p. 425.
- ²⁰P. Schiffer and I. Daruka, *Phys. Rev. B* **56**, 13 712 (1997).
- ²¹R. Moessner and A. J. Berlinsky, *Phys. Rev. Lett.* **83**, 3293 (1999).
- ²²H. Zhang, J. W. Lynn, W.-H. Li, and T. W. Clinton, *Phys. Rev. B* **41**, 11 229 (1990).